# Center for Lifespan Psychology

Director: *Ulman Lindenberger*

## Research Scientists

*Viktor Müller*
*Ulman Lindenberger*

*Caroline Szymanski* (until 07/2018)

## Research Project 5: Interactive Brains, Social Minds

In everyday life, people often coordinate their actions. Common examples include walking with someone at a set pace, playing team sports, dancing, playing music in a duet or group, as well as a wide range of social bonding behaviors, such as gaze coordination between mother and infant or between partners. The developmental and social significance of these interpersonally coordinated behaviors is undisputed, but little, if anything, is known about the brain mechanisms that regulate their temporal dynamics. The *Interactive Brains, Social Minds* project investigates behavioral, somatic, and neural mechanisms that permit individuals to coordinate their behavior in time and space (see Figure 16).

The project has continued its major focus on analyzing electroencephalographic (EEG) data of skilled musicians playing music together. In our initial study with guitar duets, we discovered that interpersonally coordinated actions are preceded and accompanied by within-brain synchrony and between-brain oscillatory couplings (Lindenberger et al., 2009). We replicated and extended these original findings in a series of follow-up studies. In analyses of hyper-brain networks based on EEG data from a guitar quartet (Müller, Sänger et al., 2018), we found that within-brain connections tend to operate at higher frequencies (e.g., beta, gamma) than between-brain connections (e.g., delta, theta)—

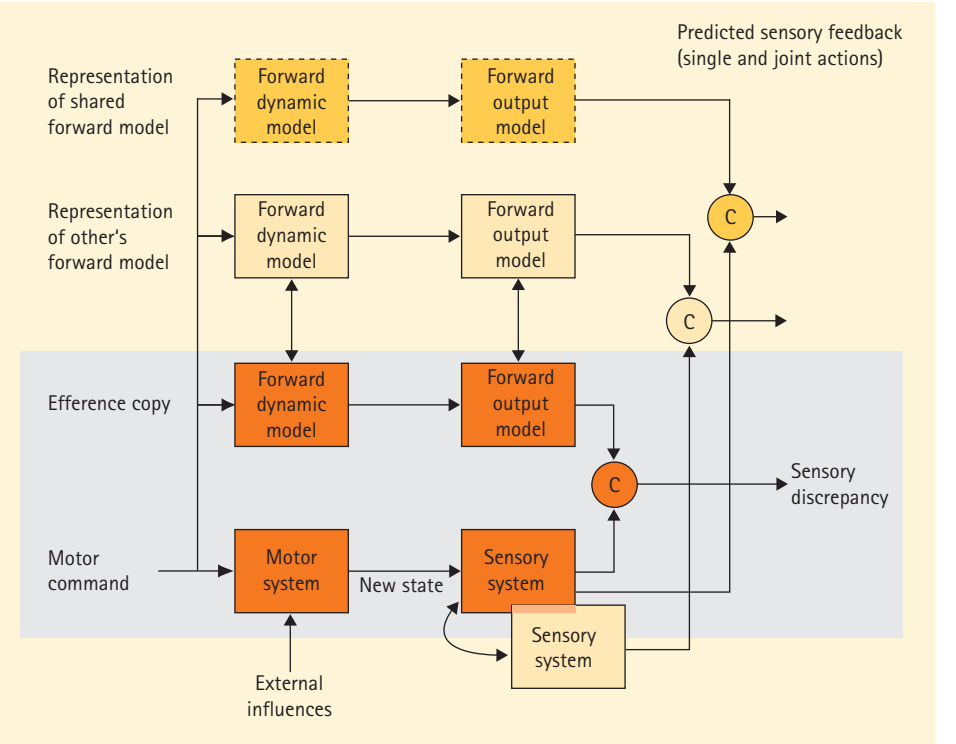


*Figure 16.* A forward model of interpersonal action coordination. Drawing on the work of Steven M. Boker, Wolfgang Prinz, Daniel Wolpert, and others, our model assumes that interpersonal action coordination is based on a set of linked representational layers. The single-person layer is shaded in gray. Individuals acting together attempt to synchronize their forward model regarding their own actions with their forward model regarding the other person's actions. Highly skilled individuals, such as dancers or musicians, may represent jointly performed activities as a unified suprapersonal action with a joint forward model and partially joint sensory feedbacks. The various representational layers of the actors are intertwined by sensorimotor feedback loops (see also Sänger et al., 2011).



### Key References

**Lindenberger, U., Li, S.-C.,** Gruber, W., & **Müller, V.** (2009). Brains swinging in concert: Cortical phase synchronization while playing guitar. *BMC Neuroscience, 10,* Article 22. https://doi.org/10.1186/1471-2202-10-22

**Müller, V., Sänger, J.,** & **Lindenberger, U.** (2018). Hyperbrain network properties of guitarists playing in quartet. *Annals of the New York Academy of Sciences, 1423*(1), 198–210. https://doi.org/10.1111/nyas.13656

**Sänger, J., Lindenberger, U.,** & **Müller, V.** (2011). Interactive brains, social minds. *Communicative & Integrative Biology, 4*(6), 655–663. https://doi.org/10.4161/cib.17934

in line with our previous results on guitar duets. Furthermore, we observed evidence for hyper-brain modules that include nodes from two, three, or even four brains (see Figure 17). We also extended our analyses to explore the dynamics of interpersonal action coordination at neural and behavioral levels of analysis during free guitar improvisation. We found that guitarists' brains were in sync with slow-frequency modulations of guitarists' acoustic signals. This provides evidence for brain–behavior entrainment reflecting temporal dynamics of coordinated music performance (Müller & Lindenberger, 2019).

We also explored the utility of hyper-frequency, hyper-brain networks in a data set of couples engaged in romantic kissing that was originally published in 2014. Oscillations in the alpha band played a central role in coordinating the two brains. Also, hyper-brain network strengths were higher and characteristic path lengths were shorter when individuals were kissing each other than when they were kissing their own hand. Between-brain strengths of theta oscillations (around 5 Hz) were reliably associated with reported partner-oriented kissing satisfaction, especially over frontal and central electrodes. Given our earlier observations of fronto-central between-brain synchronization in guitar players, we suggest that these couplings reflect cell assemblies representing movement coordination among interacting partners.

During the reporting period, we also re-analyzed the cardiac, respiratory, and vocalizing data from 11 singers and 1 conductor engaged in choir singing, originally published in 2011. We showed in greater detail how cardiac, respiratory, and voice production subsystems interact among each other both within and across singers as a function of whether a canon is sung in unison or in different voices. Notably, we found that the conductor's hand movements are synchronized with each of the three subsystems (Müller et al., 2018). With regard to network topology, we found that clustering coefficients as well as local and global efficiency were highest and characteristic path lengths, correspondingly, shortest when the choir sang a canon in parts as compared to singing it in unison. Furthermore, network metrics revealed a significant relationship to individuals' heart rate, presumably indicating arousal, and to an index of heart rate variability, reflecting the balance between sympathetic and parasympathetic activity. Based on this work, we propose that network topology dynamics capture essential aspects of group behavior and may represent a potent biomarker of social interaction dynamics (Müller et al., 2019).

In a related line of work, the project has sought to devise new EEG paradigms that are suited to observe the behavioral functions of inter-brain synchrony under experimentally more controlled conditions (Dissertation Caroline Szymanski). In one of these studies (Szymanski, Pesquita et al., 2017), participants were asked to perform a visual search task either alone or with a partner. Local phase synchronization and between-brain phase synchronization were generally higher when partners attended to a visual search task jointly than when they attended to the same task individually. Also, between-team differences in behavioral performance gain during the joint condition were associated with between-team differences in local and inter-brain phase synchronization. These results suggest that phase synchronization is a neural correlate of social facilitation that might help to explain why some teams perform better than others. A second study has tested whether same-frequency, same-phase transcranical alternating-current stimulation (tACS) is associated with greater behavioral synchrony in a dyadic drumming task than no stimulation or stimulation that differs in phase and frequency. Contrary to expectations, both stimulation conditions were associated with greater dyadic drumming *asynchrony* relative to the sham (no stimulation) condition. No influence of hyper-tACS on behavioral performance was seen when participants were asked to drum separately in synchrony to a (Szymanski, Müller et al., 2017). These results indicate that the interactions between externally triggered and intrinsically generated frequencies and phases require further theoretical and empirical work.

**Key References**


**Müller, V., Delius, J. A. M., & Lindenberger, U.** (2019). Hyper-frequency network topology changes during choral singing. *Frontiers in Physiology, 10,* Article 207. https://doi.org/10.3389/fphys.2019.00207

**Müller, V., Delius, J. A. M., & Lindenberger, U.** (2018). Complex networks emerging during choir singing. *Annals of the New York Academy of Sciences, 1431* (1), 85–101. https://doi.org/10.1111/nyas.13940

**Müller, V., & Lindenberger, U.** (2014). Hyper-brain networks support romantic kissing in humans. *PLoS ONE, 9* (11), Article e112080. https://doi.org/10.1371/journal.pone.0112080

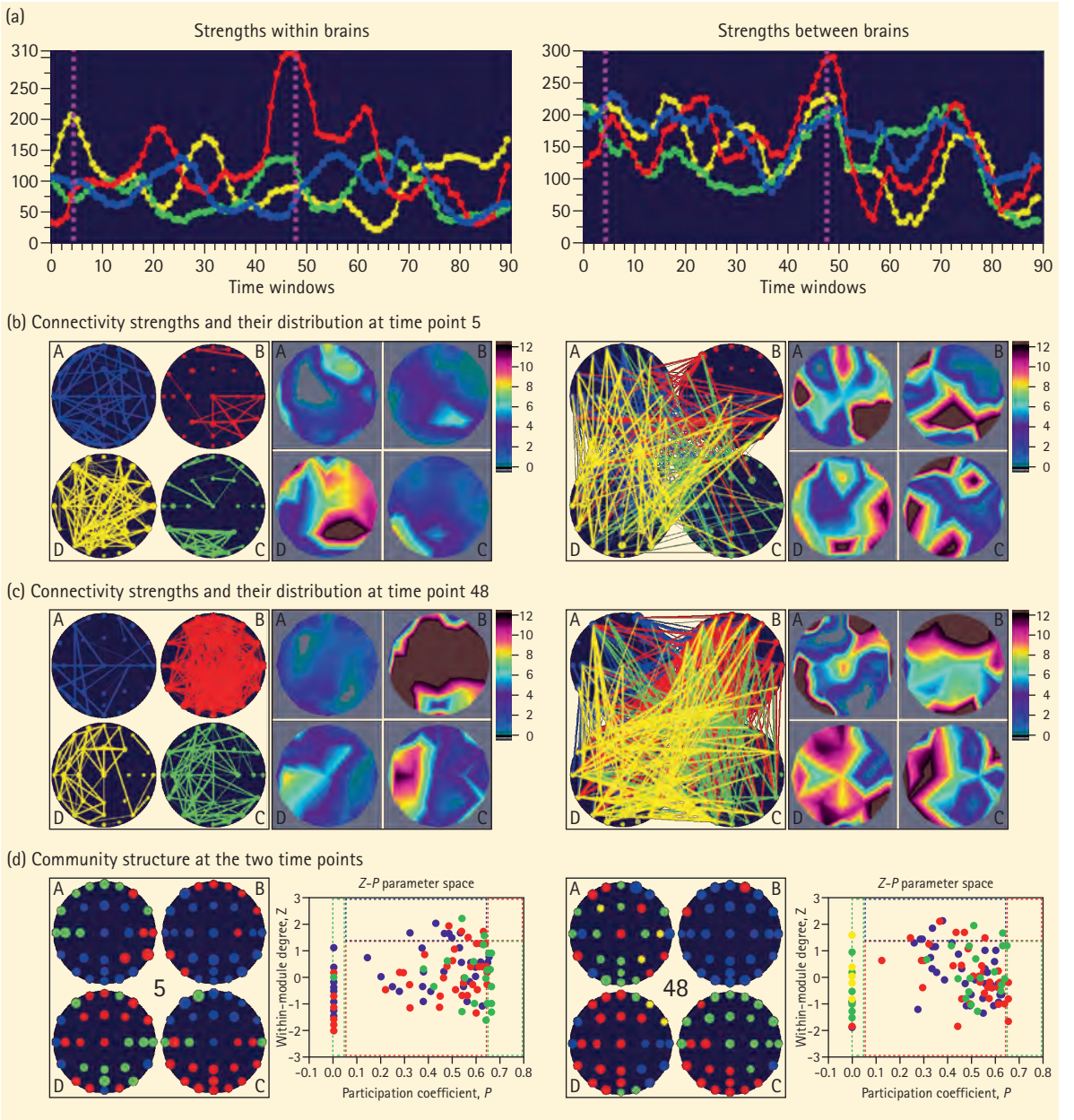


*Figure 17.* Coupling strengths and connectivity brain maps while playing guitar in a quartet, assessed in a moving window approach. (a) Time course of within- and between-brain out-strengths in the four guitarists. (b) Brain connectivity maps and distribution of strengths within (left panel) and between (right panel) the brains at time window 5. (c) Brain connectivity maps and distribution of strengths within (left panel) and between (right panel) the brains at time window 48. Note that the colors in (a) to (c) correspond to the different guitarists. The time windows are indicated by dotted vertical lines in (a). Strong within- and between-brain connectivity is evident in the first time window (5), when guitarist D (shown in yellow) is playing alone. In the second time window (48), when the musical theme begins to be repeated, strong within- and between-brain connectivity is evident in guitarist B (shown in red). (e) Modularity or community structures of hyper-brain networks with *Z-P* parameter space across the same time windows. Modules are coded by color. Note that most modules share nodes across two, three, or even four brains (adapted from Müller, Sänger, & Lindenberger, 2018).

## Research Project 6: Brain Imaging Methods in Lifespan Psychology

### Research Scientists

*Nils C. Bodammer*

*Ulman Lindenberger*
*Naftali Raz*
*Davide Santoro*

Research on human development seeks to delineate the variable and invariant properties of age-graded changes in the organization of brain–behavior–environment systems. In this vein, various magnetic resonance imaging (MRI) modalities, including magnetic resonance spectroscopy (MRS), have become indispensable, as they allow for the noninvasive assessment of brain function, anatomy, microstructure, and metabolism.

The two main goals of the *Brain Imaging Methods* project are to: (a) ascertain and improve the measurement quality of standard brain imaging protocols at the Center; and (b) complement the standard imaging repertoire by advanced sequences with enhanced interpretability that hold promise in elucidating structural changes and physiological mechanisms related to maturation, learning, and senescence. In pursuing these goals, the project serves as a resource to other projects interested in imaging (e.g., Bender et al., 2018; Dahl et al., 2019; Keresztes et al., 2017; Kleemeyer et al., 2017; see Figure 18).

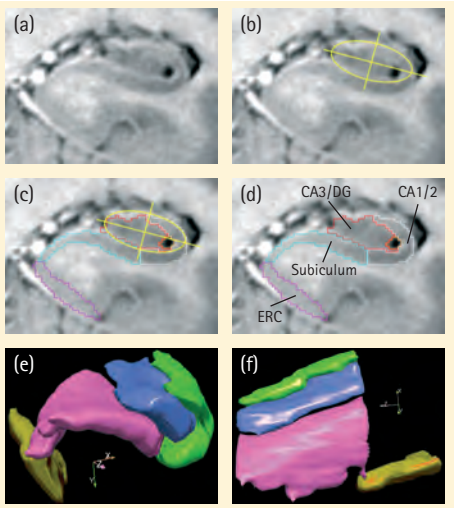


*Figure 18.* Illustration of the anatomic-geometric heuristic for manual morphometry. (a) A representative slice of anterior hippocampal (HC) body following the visualization of the uncal sulcus. To facilitate tracing, the $T_2$-weighted contrast has been inverted to mimic a $T_1$-weighted image. (b) Placement of the ellipse and bisecting lines (the major and minor axes of the ellipse). (c) The minor axis bisecting the ellipse marks the point from which a vertical line is dropped to create a boundary separating the subiculum from CA1/2, and CA 1/2 from CA3–4/DG, as shown in (d). Bottom: 3-D illustrations of sagittal (e) and oblique coronal (f) views of manual subfield labeling in the HC body from one participant (adapted from Bender et al., 2018).



*Structural and quantitative MRI methods* occupy a central place in the project. During the reporting period, the project has focused on: (a) $T_1$-mapping by means of an MP2RAGE acquisition protocol to obtain estimates of laminar myelination across the cortical sheet; (b) myelin water fraction (MWF) imaging, which maps the fraction of short $T_2$ relaxation rates quantitatively and appears to yield more valid estimates of myelin than other widely used methods; (c) advanced methods in high angular resolved diffusion imaging (HARDI), from which maps of water diffusion in brain tissue can be deduced that permit estimates of local axonal orientation and thereby enable the identification of particular fiber tracts in white matter; and (d) neuromelanin-sensitive high-resolution imaging of the brainstem to determine the individual position and extent of the loci coerulei (Dahl et al., 2019).
*Functional MRI and MRS* are used to provide maps and spectra of brain activity during task performance or at rest. The project takes special interest in: (a) functional imaging with high spatial or temporal resolution by exploiting multiband echo-planar imaging (MB-EPI) acquisition strategies; and (b) task-related, time-resolved applications of proton MRS, with a focus on glutamate. Work on MR spectroscopy and MWF imaging, on the one hand, and on $T_1$ mapping, on the other, has been done in collaboration with Jeffrey A. Stanley (Wayne State University, Detroit, USA) and José P. Marques (Donders Institute, Radboud University, Nijmegen, Netherlands), respectively. For more information about the Institute's MRI facility, see p. 298.

### $T_1$ Mapping Using MP2RAGE With $B_1$ Map Corrections

The longitudinal relaxation time $T_1$ in the cortex is affected by the myelin content in the laminae. $T_1$ mapping offers a noninva-

#### Key Reference

**Bender, A. R., Keresztes, A., Bodammer, N. C., Shing, Y. L., Werkle-Bergner, M., … Kühn, S., Lindenberger, U.,** & **Raz, N.** (2018). Optimization and validation of automated hippocampal subfield segmentation across the lifespan. *Human Brain Mapping, 39*(2), 916–931. https://doi.org/10.1002/hbm.23891

**Key References**

Arshad, M., Stanley, J. A., & **Raz, N.** (2017). Test-retest reliability and concurrent validity of in vivo myelin content indices: Myelin water fraction and calibrated $T_1w/T_2w$ image ratio. *Human Brain Mapping, 38*(4), 1780–1790. https://doi.org/10.1002/hbm.23481.

**Santoro, D.,** Rivoire, J., Meise, F., Terekhov, M., Salhi, Z., Gast, K., & Schreiber, L. M. (2011). Three-dimensional mapping of the B1 field using an optimized phase-based method: Application to hyperpolarized $^3$He in lungs. *Magnetic Resonance in Medicine, 65*(4), 1166–1172. https://doi.org/10.1002/mrm.22683

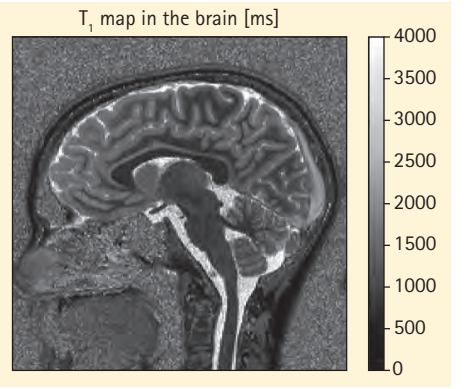


*Figure 19.* Typical $T_1$ map of a child's brain (1 slice out of a 3D volume) obtained with our protocol using MP2RAGE and $B_1$ map correction.



sive method to determine cortical structures and their changes over time. We have been developing a new protocol that makes use of multiple MP2RAGE sequences developed by José Marques and colleagues for the accurate estimation of high-resolution $T_1$ maps in the full brain. We have chosen tailored paired values for the inversion times to cover the whole range of $T_1$ values in the brain. The resulting $T_1$ map is then corrected by a $B_1$ map to cancel hardware imperfections and radio frequency inhomogeneities across the brain (see Figure 19). The $B_1$ mapping method used (Santoro et al., 2011) was optimized in-house for our studies. The full protocol for a 1 mm isotropic $T_1$ map of the full brain of children takes about 16 minutes, with work in progress to reduce its duration.

**Myelin-Water Fraction Imaging (MWF)**

Based on a time series of $T_2$-weighted MR images with increasing echo-times acquired by a 3D GRAdient and Spin-Echo (GRASE) sequence, MWF imaging evaluates the transversal relaxation in a multiexponential manner by applying a nonnegative least squares (NNLS) fitting algorithm. The fraction of short $T_2$s (< 40 ms) provides an estimate of the portion of water molecules located between myelin sheaths, presumably reflecting the degree of myelination within white matter (Arshad et al., 2017).

**High Angular Resolved Diffusion Imaging (HARDI)**

Diffusion imaging captures the movement of water molecules, termed diffusion. Diffusion in tissue is hindered by cell membranes. Therefore, the orientation-dependent diffusion profiles provide information about tissue microstructure. For instance, when water molecules are observed in myelinated neuronal fibers, their diffusion is hampered less along than across fiber tracts. Hence, principal diffusion directions can be identified with the orientations of axonal tracts. Special MR protocols sensitized to the diffusion of water molecules in tissue allow to measure such diffusion orientation profiles. In his thesis, Maximilian M. Wichmann (2018), a master's student in our project, determined the precision and estimates of accuracy of the analyzed principal diffusion directions as a function of the diffusion-sensitizing gradient scheme and the model to describe diffusion profiles. The tensor model was significantly outperformed by two competing models (sticks-and-ball, constrained spherical deconvolution).